Microstructure Study on Barnett Shale

A Thesis

Presented to

the Faculty of the Department of Earth and Atmospheric Sciences

University of Houston

In Partial Fulfillment

of the Requirements for the Degree

Master of Science

in

Geophysics

By

Di Chen

May 2012

Microstructure Study on Barnett Shale

_____

Di Chen

APPROVED:

_____

Dr. Evegeni M. Chesnokov, Chairman

Department of Earth and Atmosphere Sciences

_____

Dr. Michael Murphy

Department of Earth and Atmosphere Sciences

_____

Dr. Yasser M. Mettwally

Department of Earth and Atmosphere Sciences

_____

Dr. Dileep K. Tiwary

Chevron Corporation

_____

Dean, College of Natural Science and Mathematics

ACKNOWLEDGEMENT

I would like to express my deepest gratitude to Dr. Evgeni Chesnokov for all his classes and advice on my research work at University of Houston. His teachings and guidance helped me immensely. It is he who made my 2-year study of geophysics thorough and systematic.

Special thanks to my committee members. Thanks to Dr. Michael Murphy for significantly enriching my geology background, and thanks to Dr. Dileep K. Tiwary, from Chevron Corporation, for his insightful suggestions on my research and career. I am also grateful to Dr. Yasser Metwally for his help on my microstructure study of Barnett Shale.

Thanks to the entire Department of Earth and Atmosphere Sciences at the University of Houston for all their willingness to help during my Master study period. As I am one of the Teaching Assistants, I am grateful to Dr. Julia Wellner, Dr. Jinny Sisson, and all the other TAs with whom I worked. It is you all that made the school feel like a warm family.

Last but not the least, I would like to express my gratitude to all my friends at University of Houston, especially: Tao Jiang, Aslan Gassiyev, Kefei Lu, and Yiduo Liu. Thanks, Long Chang, for training me to use the FIB-SEM. Thanks to Denet Pernia-Huang for instructing me on TOC experiments. You are the people who inspired me to

conquer my fears and step forward. Thank you so much for all the support and encouragement along the way.

Microstructure Study on Barnett Shale

An Abstract of a Thesis

Presented to

the Faculty of the Department of Earth and Atmospheric Sciences

University of Houston

In Partial Fulfillment

of the Requirements for the Degree

Master of Science

in

Geophysics

By

Di Chen

May 2012

ABSTRACT

This thesis presents the discussion of the microstructure of the Barnett Shale as studied using the combined technology of the Focus Ion Beam (FIB) and Scanning Electron Microscope (SEM). This study mainly focuses on 12 core samples from the Barnett Shale reservoir. Theoretical models, which could be used to calculate the effective stiffness tensor of gas shale, require different types of input data. I used the FIB-SEM to find support for input parameters required for theoretical models, such as cracks connectivity, aspect ratio, mineral alignment, porosity, etc., since the pictures taken from the FIB-SEM offer us a way to analyze what is going on in the nano – scale world. This paper also discusses obtaining the other input data using various methods. X-ray Diffraction (XRD) was used to get the mineral compositions. The result of XRD indicates that the core samples are mainly comprised by quartz and clay minerals. Total Organic Carbon (TOC) contents of 12 samples were measured with the average around 4.5%.

Contents

List of Figures

List of Tables

Chapter 1:

Introduction

Recently, gas shale reservoirs have been showing their promises as a great source of stable, secure natural gas that have the ability meet the increasingly growing demand for energy. According to a survey from U.S. Energy Information Administration in 2010, dry shale gas production has increased to 4.8 trillion cubic feet, which equals 23 percent of total U.S. dry natural gas production. Moreover, by the end of 2009, wet shale gas had increased to almost 60.64 trillion cubic feet, which comprises more or less 21 percent of overall U.S. natural gas reserves.

Ranked as the 2nd most producible reservoir among onshore natural gas reservoirs, located next to the New Mexico, the Barnett Shale has been proven to contain 43.4 trillion cubic feet of shale gas (U.S. Energy Information Administration, 2010), which has the potential to offer enough natural gas to power all Texans' homes for nearly 200 years (Railroad Commission of Texas, 2012). Moreover, increasingly more gas shale plays are believed to exist and are gradually being discovered. In the year 2008, the production of natural gas from the Barnett Shale reservoir had already contributed more than $133 billion to the state of Texas, and had helped with the creation of over a million jobs (Energy from Shale, 2010).

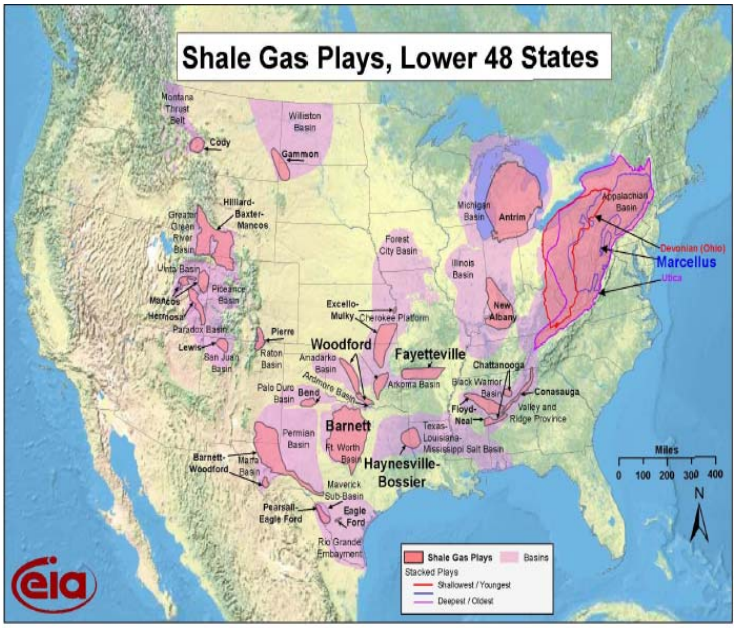

Source: Energy Information Administration based on data from various published studies.
Updated: March 10, 2010

Figure 1.1: Locations of shale gas plays in the lower 48 states. (The upper one) Locations were updated March 10th, 2010. (The lower one) Updated May 10th, 2011, prospect plays are indicated (circled by red lines) (U.S. Energy Information Administration, 2010 & 2011).

Without even mentioning the other higher production unconventional reservoirs, the Barnett Shale plate alone has already produced 1.9 TCF of natural gas through Jan. – Dec., 2011, accounting for 31% of the entire Texas production (Railroad Commission of Texas, 2012).Thus, both from the prospect of economy and the energy future of our world, we believe that the scientific research on gas shale is without a doubt meaningful.

Modern industry has a strong willingness to explore gas shale due to both scientific and economic concerns. Figure 1.2 shows the active permits and wells carried on the Barnett Shale reservoir. Unfortunately, shale is considered as an anisotropic medium or Transversely Isotropic (TI) medium with extremely low permeability, which is usually around micro Darcy range (Tiwary, 2007). Therefore it is not easy to extract gas or oil out of the reservoirs. With the help of developing technology such as hydraulic fracturing and horizontal drilling, the exploration of gas shale is becoming more practical (Schieber, 2010).

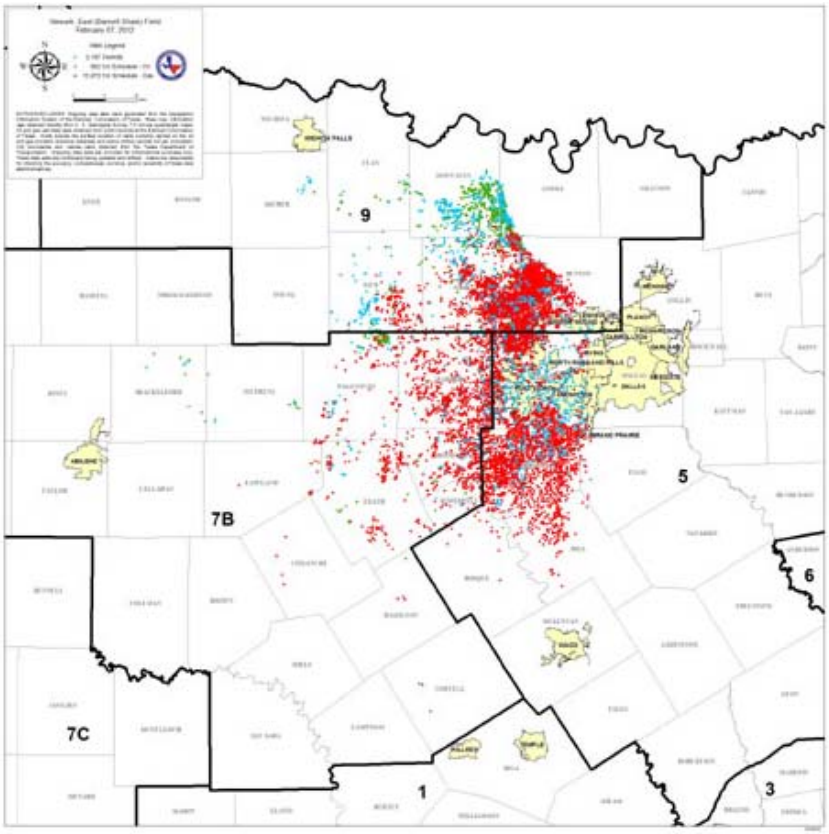

Figure 1.2: Map of active permits and wells currently carried on the oil proration schedule and gas proration schedule database. Green spots – oil wells; Red spots – gas wells; Blue spots – drilling permits (Railroad Commission of Texas, updated Feb. 17th, 2012).

In this thesis, I have worked on the core samples from Barnett Shale reservoir, discussed a way to analyze this special kind of nano-sized system, and acquired the input data for a theoretical model. In Chapter 2, the geologic related background information about the working samples such as stratigraphic features, samples' locations, and also microstructures pictures, etc. is presented.

Obviously, mineral composition and microstructure control the elastic and transport properties of gas shale (Tiwary, 2007). In order to get a better understanding of it, we would like to take a look at an overview of the microstructure of the Barnett Shale by using the combination of the Focus Ion Beam and Scanning Electron Microscope (FIB-SEM). This type of investigation provides a basic understanding of gas shale microstructure, which will have important implications on not only modeling elastic behavior and fluid flow in gas shale but also how and where gas is stored in the shale. The use of FIB-SEM and its results is discussed in more detail in Chapter 3.

Furthermore, Chapter 3 discusses the analyses of mineral composition resulting from X-Ray Diffraction (XRD), which is the most comprehensive way to identify minerals (Stanjek and Halser, 2004). Additionally, geochemical methods were used to obtain the Total Organic Carbon (TOC) content.

Chapter 4 presents all the results acquired from the various methods presented in Chapter 3. Also, there is a discussion about the advantages and disadvantages of FIB-SEM. The accuracy of XRD spectrum interpretation and TOC weight percent analysis are discussed as well.

The thesis ends with conclusions in Chapter 5, which summarizes the importance of studying gas shale and reviews different methods that have been used to obtain the different types of input data.

Chapter 2:

Barnett Shale – Sample Addressed

This chapter contains the basic knowledge of gas shale and samples that I worked on. First of all, the different definitions of gas shale from different aspects are reviewed. Second, the drilling history of Barnett Shale as well as its production records is presented.

Also, an introduction to samples' backgrounds is provided in detail. Details include the location, depth, and other geologically related characters, and are described by several visual aids such as a stratigraphic map and a depth map.

2.1 Definition of Gas Shale

Usually gas shale is known as an anisotropic medium within fine-grained sedimentary rock. It is considered a Transversely Isotropic (TI) medium more often (Tiwary, 2007), since it has apparently paralleled layers that can be seen under the FIB-SEM as shown in Figure 2.1. However, in Figure 2.1, to the right, the symmetry of this anisotropic medium is tilted by several degrees from the vertical direction. Furthermore, gas shale is a porous medium with nano-sized pores and nano-Darcy permeability, which is extremely low compared to those of conventional reservoirs.

According to Schmoker (2002), gas shale reservoirs were treated as an unconventional, continuous petroleum system caused by the accumulation of hydrocarbons. However, when talking about production, most hydrocarbons are found in low-matrix-permeability rocks which are fracture permeability dependent (either natural or as a result of stimulation). Moreover gas shale reservoirs contain large amounts of hydrocarbons but have low gas recovery factors.

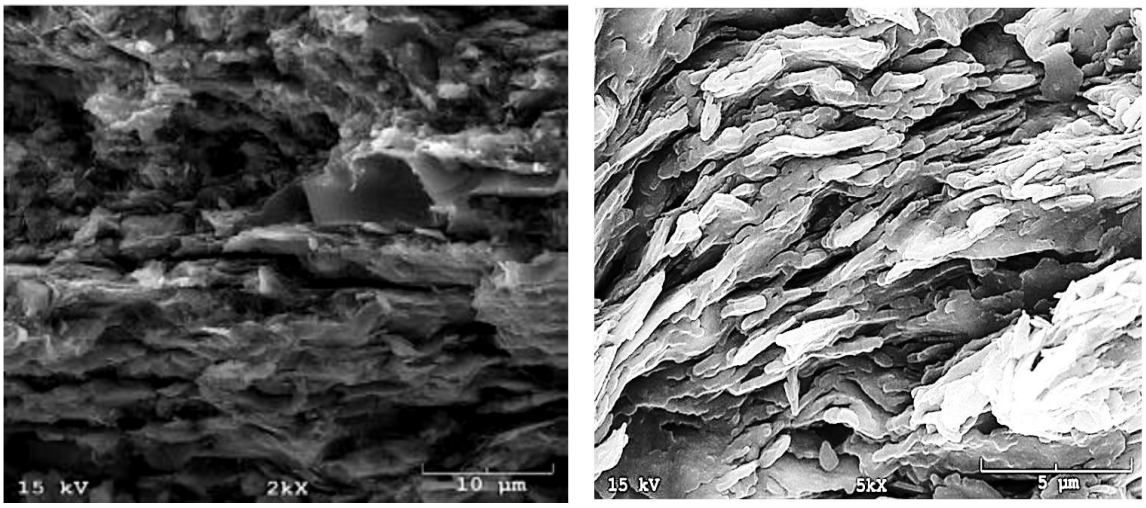

Figure 2.1: To the left, the fractures' orientation is paralleled to the beddings; to the right, minerals' alignment is paralleled to the bedding as well (Metwally and Chesnokov, 2011).

Within the gas shale, the free gas is stored in the pore space, usually in the carbonate pores (Figure 2.2). In this FIB-SEM picture, the grey area surrounded is the clay minerals. The vertical lines at the bottom are not the real ones, they are the charging affects caused by the organic content and the electron beam. Also, the pores' sizes range roughly from 0.05 µm to 0.4 µm, based on the 1µm scale bar. It is these 10-9m scale pores that make the system more complex and even more difficult to extract natural gas out of gas shale.

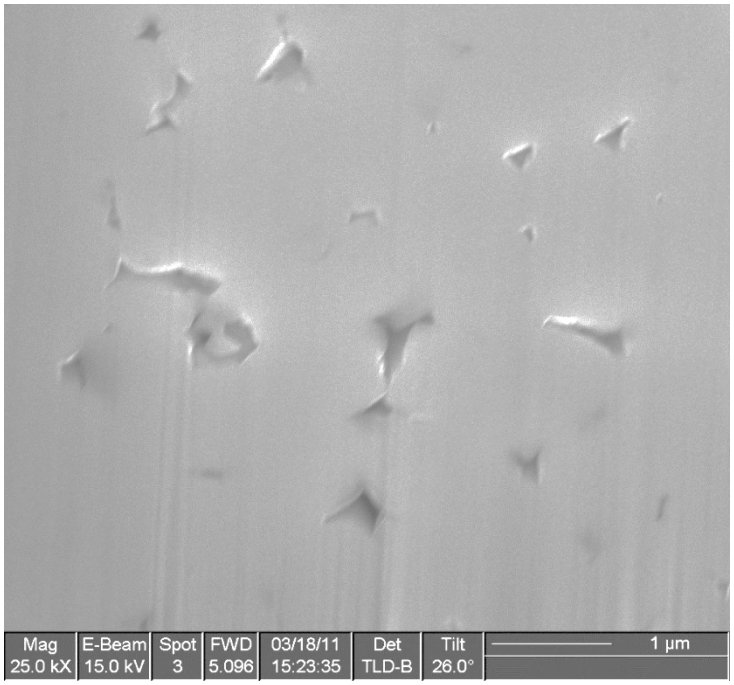

Figure 2.2: Carbonate pores seen under FIB-SEM.

Thirdly, the Barnett Shale contains a large amount of organic matter, found in kerogen. Meanwhile, we found it does contain considerable amount of porosity within the kerogen content as shown in the FIB-SEM picture (Figure 2.3). We believe that the absorbed gas is stored in kerogen.

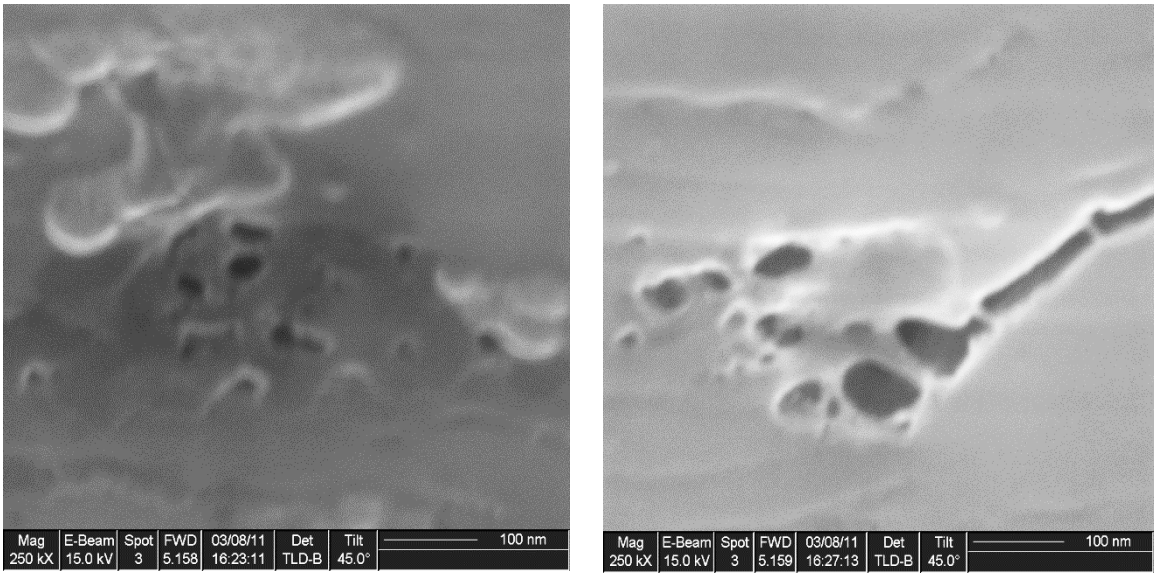

Figure 2.3: Organic pores seen under FIB-SEM. A large amount of porosity is observed. To the right, the picture shows not only the pores but also the pores connected with a small channel.

2.2 Drilling and Production History of Barnett Shale Reservoir

The Barnett Shale was first explored on October 1981. According to the RRC Records as of March 5, 2012, there are 15,731 gas wells in total that have been drilled in Barnett Shale Field. There are another 3,112 permitted locations ready to be produced.

There are 23 counties are engaged in production. In alphabetical order, they are Archer, Bosque, Clay, Comanche, Cooke, Coryell, Dallas, Denton, Eastland, Ellis, Erath, Hill, Hood, Jack, Johnson, Montague, Palo Pinto, Parker, Shackelford, Somervell, Stephens, Tarrant, and Wise (Railroad Commission of Texas, 2012).

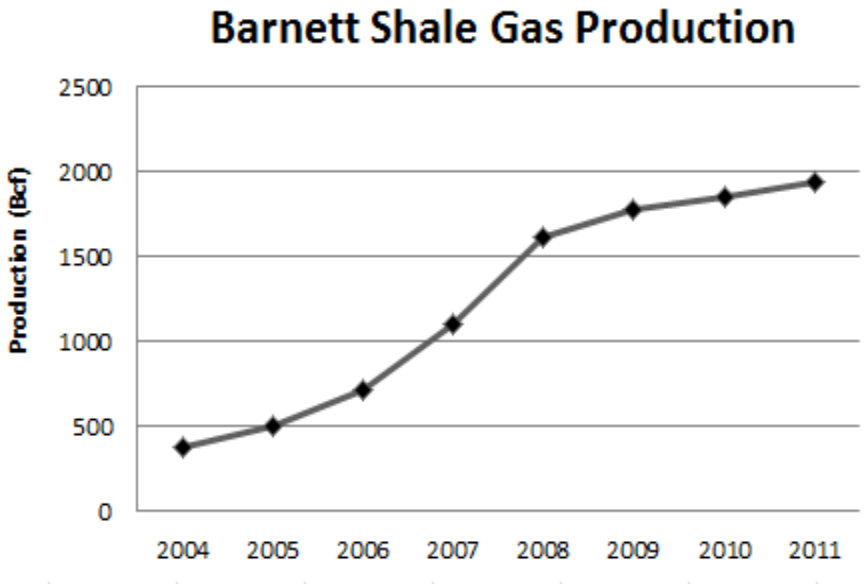

Figure 2.4: The gas production of Barnett Shale summary (Data collected by Railroad Commission of Texas, updated Feb. 17th, 2012).

The graph above (Figure 2.4) indicates the total gas production from gas well drilling in the Barnett Shale Field. In the year 2011, the production contributed 31 percent to the entire Texas Production (Railroad Commission of Texas, 2012).

There are a total of 237 operators in the Barnett Shale Field (Railroad Commission of Texas, 2012). The top 10 operators for the year 2011 are listed here, ranked by their gas production from gas wells (See the Table 2.1).

Table 2.1: List of major operators in the Barnett Shale Field, ranked by gas production from gas wells (Data courtesy of Railroad Commission of Texas, 2012).

Operator Name	Operator No.	Gas Well Gas (Mcf)
Devon Energy Production Co, L.P.	216378	481,862,641
Chesapeake Operating, INC.	147715	448,890,759
Xto Energy, INC.	945936	305,236,654
EOG Resources, INC.	253162	168,269,705
Quicksilver Resources, INC.	684830	151,227,988
Carrizo Oil & Gas, INC.	135401	55,965,880
Encana Oil % Gas (USA), INC.	251691	55,915,739
Williams Prod. Gulf Coast, L.P.	924558	32,699,717
Enervest Operating, L.L.C.	252131	27,511,530
Burlington Resources O&G CO, LP	109333	25,182,260

2.3 General Geologic Setting of Barnett Shale

The Barnett Shale, an onshore nature gas field, consists of Devonian-Mississippian age rocks (323–354 million years ago) (Pollastro et al., 2003b), and was named after 19th Century settler John W. Barnett. It is located in the Bend Arch-Fort Worth Basin in the northeast of Texas covering at least 6,458 square miles (~16,730 km^2), and containing approximately 39Tcf of natural gas (U.S. Geological Survey, 2010). Most plays are about one mile and a half below several North Texan cities, some of which sustain high population levels. For instance, the Dallas/Fort Worth Area is included (Energy from Shale, 2010).

The Barnett Shale gas system, a self-contained source-reservoir system, has generated large amounts of natural gas in over 20 key productive areas in north Texas counties (Jarvie, et al., 2007). It has been proven to be a high-thermal-maturity shale basin (Jarvie et al., in press).

In fact, geologists knew about Barnett Shale for quite a long time before the development of horizontal drillings and the increase of natural gas prices, which have made exploration and production of natural gas a reality (Pollastro et al., 2003a).

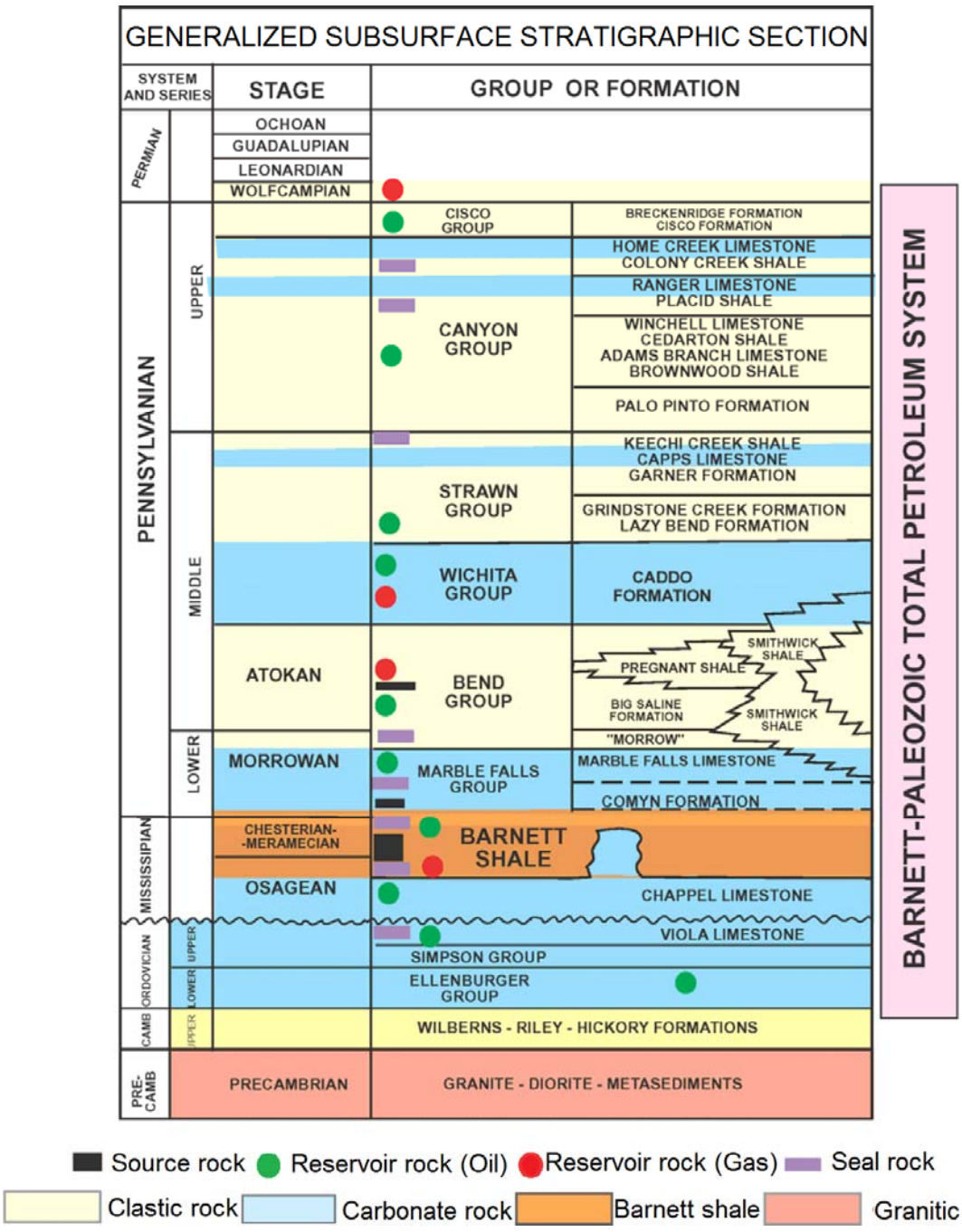

Figure 2.5: Stratigraphic map of Barnett Shale from the Bend Arch – Fort Worth Basin (Pollastro et al., 2003b)

2.4 Samples Introduced

In total, we have 12 core samples which are classified into 6 sets corresponding with 6 different wells. Each set has 2 samples taken from the same well, but at 2 different depths. Moreover, these 6 wells correspond to 5 different counties (Figure 2.6).

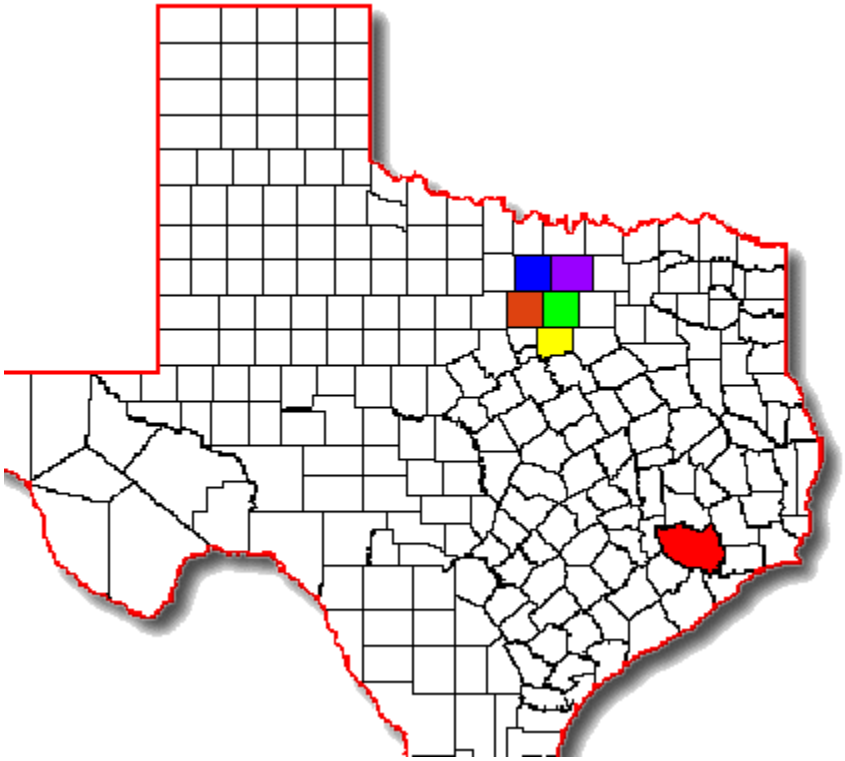

Figure 2.6: Locations of the 6 different wells spread in 5 counties.

SC (I, II) & AS (V, VI) **JR (III, IV)** **BR (VII,VIII)**

ST (IX,X) **RCT (XI,XII)** **HOU (Harris)**

The depths of Barnett Shale are commonly estimated to be around 6500-8500ft (~1980-2590m). The average thickness is 350ft (~107m) within the core areas, with the actual values varying from 50ft (~15m) or less to more than 1000ft (~305m) throughout the entire basin (Pollastro, et al., 2003a; Pollastro, et al., 2003b; Montgomery et al., 2005).

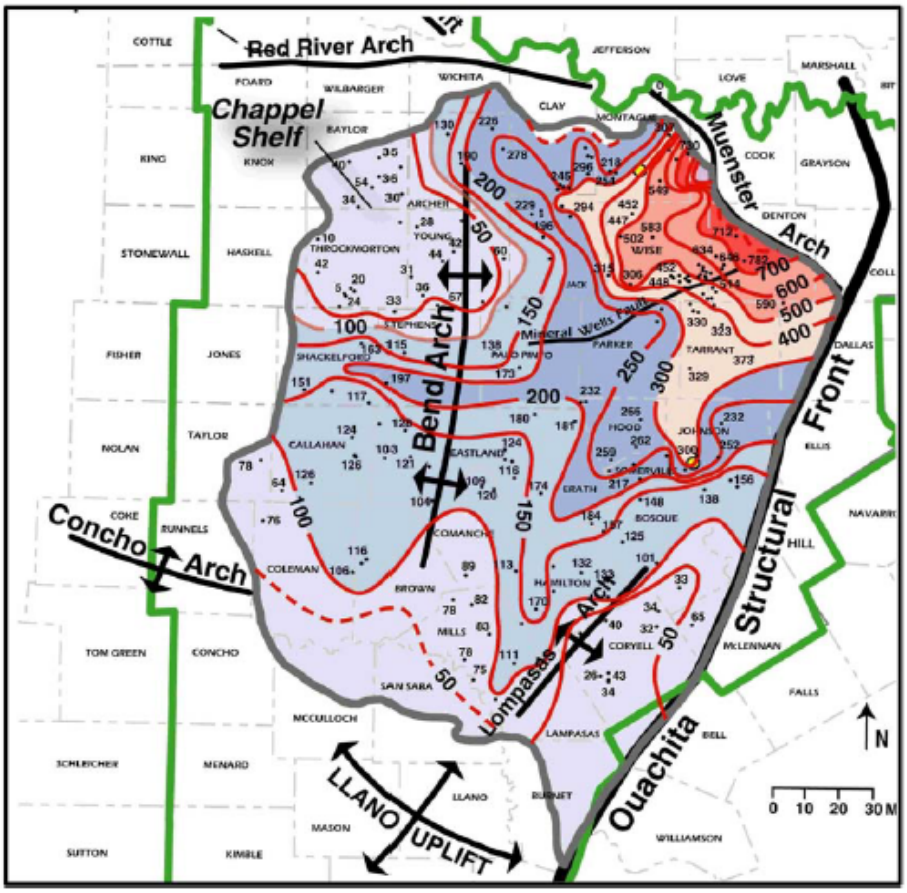

Figure 2.7: Thickness Map of Barnett Shale, Bend Arch-Fort Worth Basin, from U.S. Geological Survey. The Green line shows the USGS Province 50 Boundary – Bend Arch-Fort Worth Basin. The Grey line indicates geographic extent of Barnett Shale. Contour intervals for isopach map are 50ft (~15.2m) from 0 to 300ft (~91.4m), and 100ft (~30.5m) from 300ft (~91.4m) to 1,000ft (~304.8m).

For our 12 samples, ST(ix) is taken from the most shallow depth at 5105ft (1,556m), and RCT(xii) is from the deepest depth at 7830ft (2,387m). All in all, the variability of depth is within 2750ft (838m). Figure 2.7 indicates the thickness of Barnett Shale reservoir. The green line circling the region shows geographic area, while the contour lines show the thickness trend from the southwest to the northeast, along where the reservoir is getting thicker and thicker.

All the previous geochemical studies on Barnett Shale were summarized by Pollastro, et al., 2007. Their paper stated that the average TOC values of the Barnett Shale vary between approximately 4.0 and 5.0 wt%, while the actual value could be as much as 12 wt% or even more. They were using the Vitrinite Reflectance (R0) to describe the thermal maturity of the Barnett Shale, and as far as the expectation, the maturity increases while its depth increases in front of the Ouachita Thrust Best.

Furthermore, the Barnett Shale Reservoir is mostly examined to contain the Type II kerogen, which is normally oil and gas prone (Jarvie et al., 2007), similar to our core samples. The mean TOC value of our samples is around 4~5 wt%. More details about TOC are introduced in Chapter 3.

Chapter 3:

Methodology

Chapter 3 describes all the methods used for the experiments including the Focus Ion Beam-Scanning Electron Microscope (FIB-SEM), Total Organic Carbon (TOC%) measurements, and X-Ray Diffraction (XRD) analysis. Moreover, part of the preliminary results from every experiment is presented.

FIB-SEM, a ground-breaking technology used in nano-scale investigation on gas shale, is used to do initial investigations on gas shale. Objectives and some reviews on FIB-SEM are presented in Chapter 3.1, which also contains the comparison of FIB-SEM with other previously used methods, some images results, and a pros and cons discussion.

TOC is a general index for the weight percent of organic matter. In Chapter 3, I will present the types of different kerogen, TOC% in different gas shale reservoirs, and the experimental procedures for Barnett Shale core samples.

XRD analysis offers a way to figure out the mineral composition in most cases. We can essentially get the mineralogy spectrums and interpret the wt% of different minerals. There will be further discussion of the principles of XRD analysis and its role in investigating the Barnett Shale core samples in this chapter.

3.1 Focus Ion Beam – Scanning Electron Microscopy (FIB-SEM)

3.1.1 Introduction to FIB-SEM

In order to make clear how the fluids are transported or trapped in the gas shale, which is associated with the transport and elastic properties of the rocks, it is important to first obtain a better understanding of the pore types, networks, geometry, and topology (U.S. Energy Information Administration, 2010). The Focus Ion Beam combined with the Scanning Electron Microscope offers a way of not only milling nanometer-scale surface smoothly by FIB, but also taking high-resolution pictures by SEM, simultaneously. It is the achievements of successful milling and imaging simultaneously, that have given us a series of two-dimensional (2D) images that can be stacked together and used to make a 3D reconstruction to help with building the pore network geometric model (Holzer, et al., 2004; Tomutsa, et al., 2007).

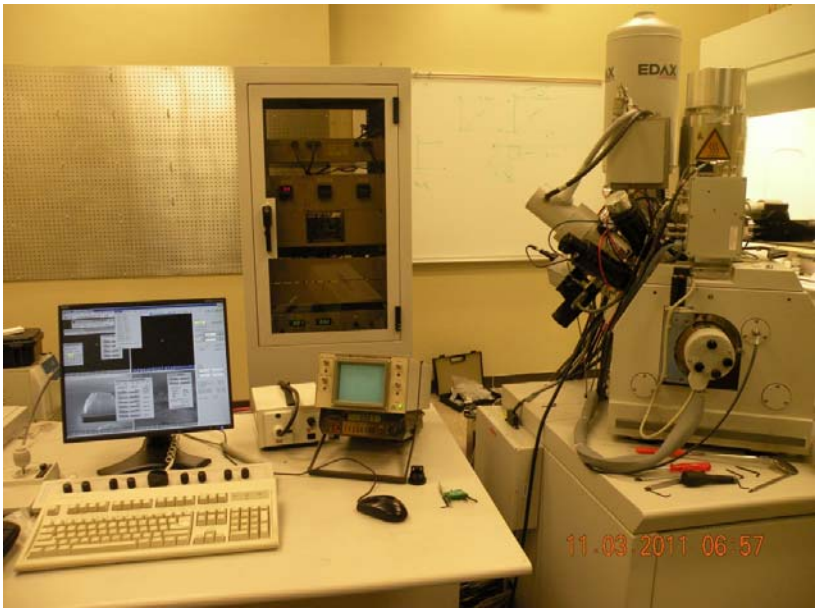

Figure 3.1: Picture of FIB-SEM facility, taken from the Nano-Lab at University of Houston

Figure 3.1 shows the outward appearance of the FIB-SEM facility. The facility is connected to a computer as a controlling platform. We can switch to use different detectors for this digital microscope in order to do the manufacture focusing, adjust the brightness and contrast of images, change the acceleration voltages of ions, etc. Meanwhile we can see the images through the microscope shown on the monitor and then decide which area is more proper to work on.

3.1.2 Dual Beam FIB-SEM Systems

This technology is supported by a dual beam system, called FIB-SEM. A simple way to describe the procedure is to explain that the FIB first makes a cross-section surface and then the SEM images the slice. The Scanning Electron Microscope (SEM) is already a well-known instrument used for investigating and imaging the microstructure of rocks, including gas shale (Chalmers et al., 2009; Wang and Reed, 2009; Schieber, 2010; Curtis, et al., 2010).

In SEM, electrons are ejected out under high acceleration voltage from an electron gun. Normally, the acceleration voltage ranges from several hundreds to 40kV (Curtis, et al., 2010). In this thesis, 15kV acceleration voltage is typically used to process the electron beam. With the help of electromagnetic lenses and scan coils, electron beams are formed. Their diameters have a threshold from tenths of nanometers to a few nanometers (Curtis, et al., 2010). Then a sample is ready to be probed with the formed electron beams.

Once we image the nano- and micro-structure of a gas shale surface, a good preparation of a sample is necessary. The Focus Ion Beam (FIB) gives a solution to prepare micro-scale features of interest specifically. It uses Ga^{+} ions, accelerated across high voltages, to bombard the sample surface. Via the function of momentum transfer, the materials on the surface will be sputtered away, and the basic milling is finished (Curtis, et al., 2010).

Moreover, there is another gas gun that contains platinum (Pt) set together with FIB (Figure 3.2 b). It allows us to deposit a strip of Pt on the surface and make the surface a homogeneous, stable, and steady planar layer for FIB to mill into. This technique reduces the undesired curtaining of artifacts greatly (Curtis, et al., 2010).

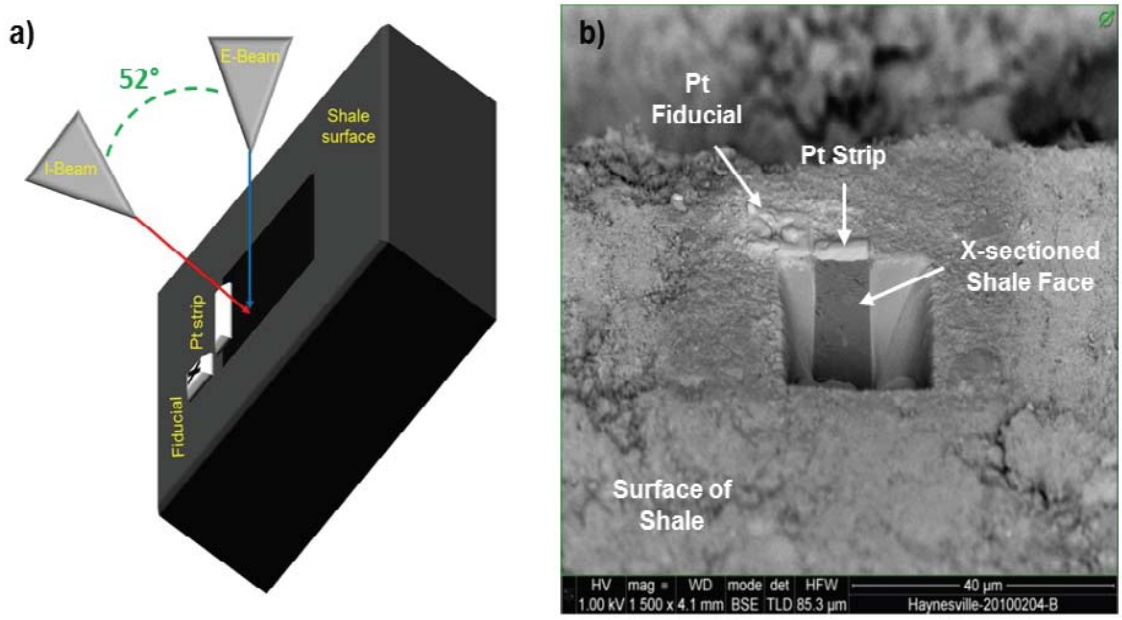

Figure 3.2: Cross-sectioning and imaging of a Haynesville sample in a dual-beam system (Curtis, et al., 2010). (a) Internal geometry of the Dual-Beam System; (b) with a Pt strip deposited, cross-sectioned shale by the I-beam, a BSE image of Haynesville shale is taken with the E-beam.

It is increasingly helpful when the FIB is arranged in the same chamber with SEM, to get the best in situ cross-sectional images serially of Barnett Shale (Curtis, et al., 2010). Figure 3.2 (a) shows the internal scheme of this dual beam system. Geometrically, the electron beam (E-Beam) is vertically built, while the ion beam (I-Beam) is set up 52º

away from it. This means that during the milling process, the I-Beam is perpendicular to the sample surface, and it causes the E-Beam to be at a position of 52º.

The reason why there is a 52º gap between these two beams is discussed as followed. According to the wedge reparation study of Cheryl Hartfield, from Omniprobe Inc. (2010), given a certain acceleration voltage, the interaction of an ion beam with a material varies as a function of material type and the angle of incidence (AOI). High AOI creates shallow depth, while low AOI makes it deeper. There are several other factors influenced by AOI, such as, the milling rate and the amount of re-deposition.

The ion beam axis is usually fixed, thus we could only change the AOI through tilting the stage. In order to create the wedge samples at high incident angels larger than 40º, a 2 degree AOI variation influenced the final depth by about 1 μm (Hartfield, 2010). Consequently, the milling recipe to achieve the geometry should be able to translate between different microscopes with no requirements on adjusting ion beam axes. Essentially, most instruments on the market put an ion beam axis between 52º to 54º for FIB-SEM system.

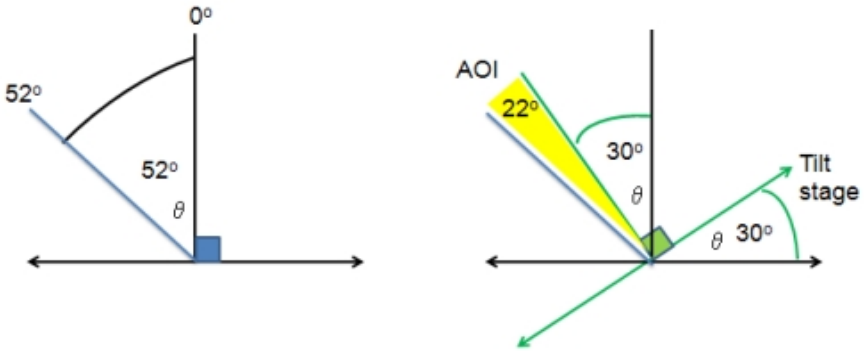

Figure 3.3: FIB Angle of Incident (AOI) impact lift-out sample success (Hartfield, 2010).

3.2 Total Organic Carbon (TOC %)

3.2.1 Kerogen Classification

Basically all sedimentary rocks have at least some levels of organic matter, although a small number of these levels abnormally occur along with an inorganic origin. Essentially, almost all profitable petroleum accumulations originated from organic matter deposited with sedimentary rocks (Nunez-Betelu and Baceta, 1994).

The capacity of a petroleum source rock is dependent on these four following factors: quantity, quality, expulsion efficiency of the source sequence, and thermal maturity of kerogen (Waples, 1979). Most often, kerogen, which is used as a nonspecific indicator of organic matter in sedimentary rocks, consists of about ~90% of organic matter in sedimentary rocks (Nunez-Betelu and Baceta, 1994). Along the burial process of the organic matter, the organic part will gradually transform into kerogen at low temperatures by biogenic reactions and decay (Pollastro, et al., 2007). Those organic contents of such sediments, which are eventually turned into the source beds of petroleum potentially, have considerable amount of kerogen (Pollastro, et al., 2007).

The quantified description index of kerogen is measured as Total Organic Carbon (TOC). It must be used when determining the petroleum generation potential of a stratigraphic unit (Nunez-Betelu and Baceta, 1994). The amount of organic hydrocarbon is practically controlled by the nature of the organic matter present in the sediment. According to the research of Dr. Nuez-Betelu's from University of Calgary, kerogen is

classified into the following four types, depending on the related source materials of organic hydrogen.

Type I kerogen corresponds with algal debris. It is mainly contained in the Triassic mudstones and siltstones of the Schei Point Formation of southern Ellesmere Island (Brooks, et al., 1992). Type I kerogen has the highest Hydrogen/Carbon (H/C) ratio compared to the other three types. Given this, type I kerogen has the highest petroleum generation potential.

Type II kerogen is derived from common marine organic matter and phytoplanktonic organism. It does not have as high H/C as type I kerogen. However, type II kerogen spreads out more common than type I kerogen. Usually it is considered to be the typical "oil" source kerogen.

The third type of kerogen corresponds to the so-called "common" terrestrial organic matter and higher land plants. Thus this type of organic matter is rich in lignin and cellulose. In spite of its terrestrial origin, type III kerogen could happen to be the dominating kerogen type in marine shale (Barker, 1974). For the core samples that I measured in this thesis, they all belong to the Type III group.

Type IV kerogen is composed of black, opaque debris of angular shape which are related with lignified precursors (Cope, 1981). It has the lowest H/C ratio and is defined as Pennsylvanian coal. Furthermore, the fourth type kerogen is related to inertinite and is often treated as "dead-carbon". It has little effectiveness in the potential of oil accumulation, however, if anything, it is used for gas (Brooks, et al., 1987).

All in all, the list below shows all the relationships between the source rock and four types of kerogen.

Table 3.1: Different types of kerogen classification (University of Calgary, 1994)

Amount of Kerogen	Dominated Kerogen Types	Deposition Types
~ 1%	I, II	Oil Source Rock
< 50%	I, II	Oil Shale
> 50%	III	Coal
~ 0%	IV	Dead-Carbon

Dirk Willen van Krevelen, chemist and professor of fuel technology at the TU Delft, Netherlands in 1950s, made the most famous graph below known as the Van Krevelen Diagram (Figure 3.4). This graph indicates the relationship of different types of kerogen. As the Hydrogen/Carbon (H/C) ratio changes, the Oxygen/Carbon (O/C) ratio changes also. Based on the graph, we see that the maturity decreases with the H/C and O/C increase simultaneously. Maturity is a concept that describes a continuous irreversible change associated with the evolution of organic matter in rocks (Nunez-

Betelu, 1994). More information extracted from Figure 3.4 shows that Type I kerogen has the highest H/C ratio while Type III contains the highest O/C ratio.

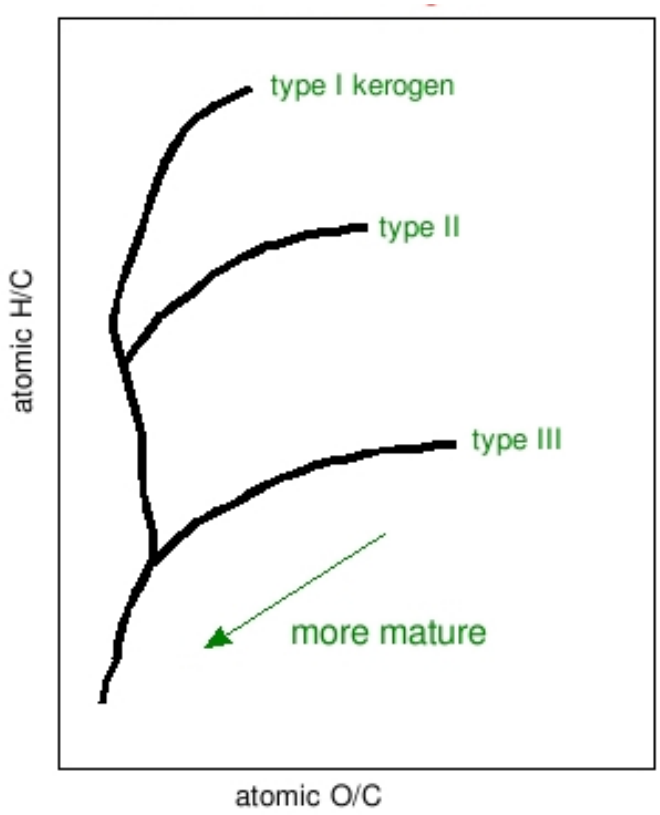

Figure 3.4: Van Krevelen Diagram

It has been proven that gas shale has on average higher TOC contents than the other sedimentary rocks, as the gas shale is defined as a continuous type of unit that commonly has high organic richness and widespread gas saturation (Jarvie, et al., 2007). We'll discuss the TOC wt% more in the next part.

3.2.2 Concept of TOC wt% and Experimental Steps

According to the chemistry definition, Total Organic Carbon (TOC) is the amount of carbon bound in an organic compound. Usually, the experiments require that the ground powder samples be measured, and the results reported in the unit of weight percent.

The principle of experimental processes is subtracting the inorganic carbon from the total carbon, which then yields TOC. Simple chemical expression is described below.

$$HCO_3^-, CO_3^{2-}, CO_2, POC \xrightarrow[carrier\ gas,\ acid]{} CO_2 + POC$$

Figure 3.5: Chemical reaction of removing the acidification.

Usually, the ground powder samples, weighing 0.09g, are contained in crystal bowls, which are extremely porous to allow the fluid to run through easily. In the geochemical laboratory, the most often used acid to remove the inorganic carbon is 6N solution, which is composed of half water and half hydrochloric acid volumetrically. After soaking in the acid solution for over 12 hours, the samples are almost acidified, and most of the inorganic ingredients are gone.

The next step is to wash the sample using distilled water. Then you must soak the samples in distilled water for another 12 hours, and wash the crystal bowls for quite several times. Before putting the crystal bowls in the facility, they need to be dehydrated. Dry the samples in the oven at 80ºC for more than 24 hours. Only when there are no

yellow spots shown on the edge of the crystal bowls, indicating that there are no organic elements involved, are the samples totally dry.

However, for the chemical reaction caused by the hydrochloric acid, the elements Cl^- run into the samples at the same time when the CO2 and H2O are being phased out. Thus it is quite common to do some correction to get the final TOC value. Essentially another 5% is added in to the original data.

Normally the burning measurement yields two kinds of items - carbon and sulfur. In this case, the sulfur contains both organic and inorganic parts, and there is no specific relationship between the amounts of carbon and sulfur according to this study.

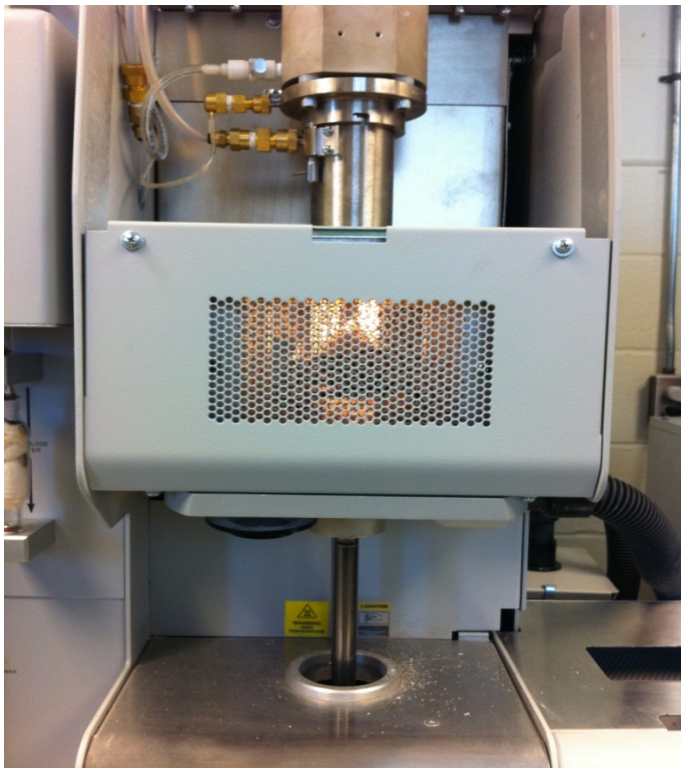

Figure 3.6: TOC sample is being measured.

The picture below (Figure 3.6) shows the spectrum in real time measurement. Usually, the TOC and sulfur are measured according to their burning time. The horizontal axis shows the time, and the vertical axis indicates the amount of carbon and sulfur detected.

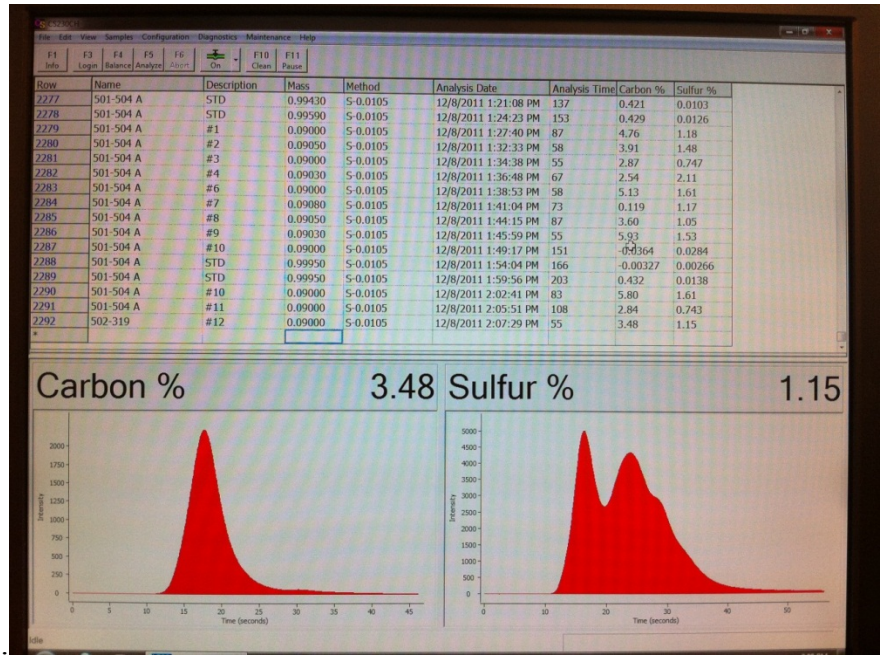

Figure 3.7: Screenshot of the results

3.3 X-Ray Diffraction (XRD)

3.3.1 Principal of XRD

Mineral contents of an unconventional reservoir are important when the operators want to perform the hydraulic fracture operations successfully; it has been concluded that quartz is the most abundant mineral in the Barnett Shale (Jarvie, et al., 2007).

The X-Ray Diffraction (XRD) analysis is the most comprehensive way to interpret the mineral composition. It is used to identify, quantify, and characterize the minerals in complex mineral assemblages (Stanjek, 2004). Its application to gas shale mineral analysis yields more information on the composition of the source rock (Jarvie, et al., 2007). The task of using XRD is therefore to identify the mineral and, if possible, to characterize the numerical content by analyzing the spectrums.

Different minerals have different atom alignment, which is usually described by the crystalline shape. Different diffractions will yield different peaks reflected on the spectrum (Stanjek, 2004). It is not easy to quantify the mineral composition only through the spectrum analyses.

Figure 3.8: The X-Ray Diffraction Analysis Facility (Picture taken at the University of Houston)

3.3.2 Common Minerals in Shale

It is the clay minerals that control the anisotropy of shale (Tiwary, 2007). The weight percent of clay minerals in my study is mostly around 20%. One of the axes in the triangle map is labeled “Others”; it includes carbonate, sulfur, and all the other minerals except quartz and clay minerals. Tables 3.3 and 3.4 present the elastic constants and density as well as the symmetry system of most common shale minerals.

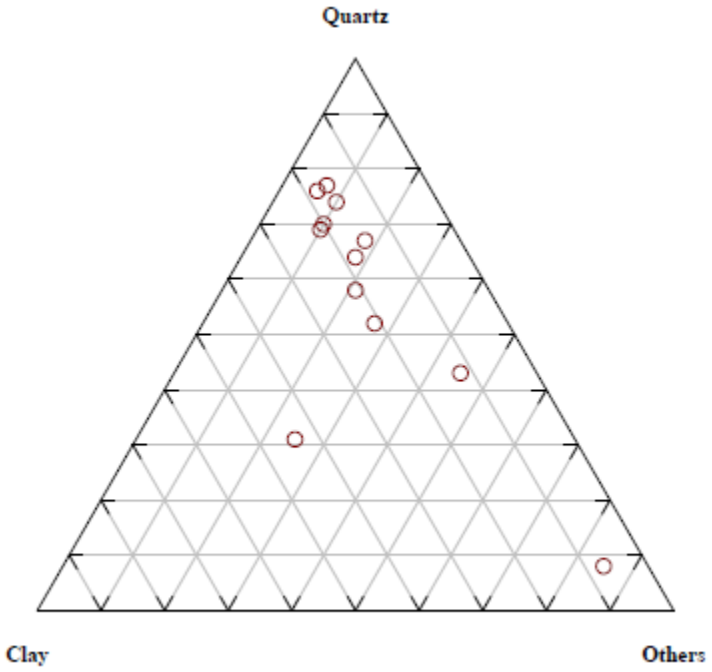

Figure 3.9: Triangle map of common minerals from 12 core samples (Data Courtesy of Yasser Metwally, UH).

Table 3.2: Elastic constants and density of commonly found minerals in shale (Data courtesy of Table 3.3 References)

C_{ij}	Quartz	Calcite	Dolomite	Albite	Clay-water	Chlorite	Kaolinite	Illite rich
C_{11}	86.0	144.5	205.0	74.0	23.66	181.76	171.52	127.387
C_{12}	7.4	57.1	71.0	36.3	12.3	56.76	38.88	48.067
C_{13}	11.91	53.4	57.4	37.6	3.05	20.34	27.11	28.369
C_{14}	-18.04	-20.5	-19.5					
C_{15}			13.7	-9.1				
C_{22}	86.0	144.5	205.0	137.5	23.66	181.76	171.52	127.387
C_{23}	11.91	53.4	57.4	32.6	3.05	20.34	27.11	28.369
C_{24}	18.04	20.5	19.5					
C_{25}			-13.5	-10.4				
C_{26}								
C_{33}	105.75	83.1	113.0	128.9	8.52	106.77	52.63	53.695
C_{34}								
C_{35}				-19.1				
C_{44}	58.2	32.6	39.8	17.2	0.83	11.41	14.76	14.411
C_{45}								
C_{46}			-13.7	-1.3				
C_{55}	58.2	32.6	39.8	30.3	0.83	11.41	14.76	14.411
C_{56}	-18.04	-20.5	-19.5					
C_{66}	39.3	43.7	67.0	31.1	5.71	62.5	66.32	39.66
ρ	2.65	2.7	3.795	2.62	2.17	2.69	2.52	2.70

Table 3.3: Most common minerals present in shale and their symmetry system and references.

Mineral	Symmetry System	References
Quartz	Trigonal	Belikov et al. (1970)
Calcite	Trigonal	Peselnick and Robie (1962)
Dolomite	Trigonal	Bass (1995)
Albite	Monoclinic	Belikov et al. (1970)
Illite-rich clay	Hexagonal	Bayuk et al. (2007b)
Chlorite	Hexagonal	Katahara (1996)
Kaolinite	Hexagonal	Katahara (1996)
Clay water composite	Hexagonal	Bayuk et al. (2007a)

Chapter 4:

Results and Discussions

This chapter presents the results obtained from different methods of experimentation. The most important part is to show the results of the Focused Ion Beam-Scanning Electron Microscope, followed by the discussions on the advantages and disadvantages of the facility. The results from TOC and XRD are presented as well.

4.1FIB-SEM Results

4.1.1 Images Analysis and Interpretation

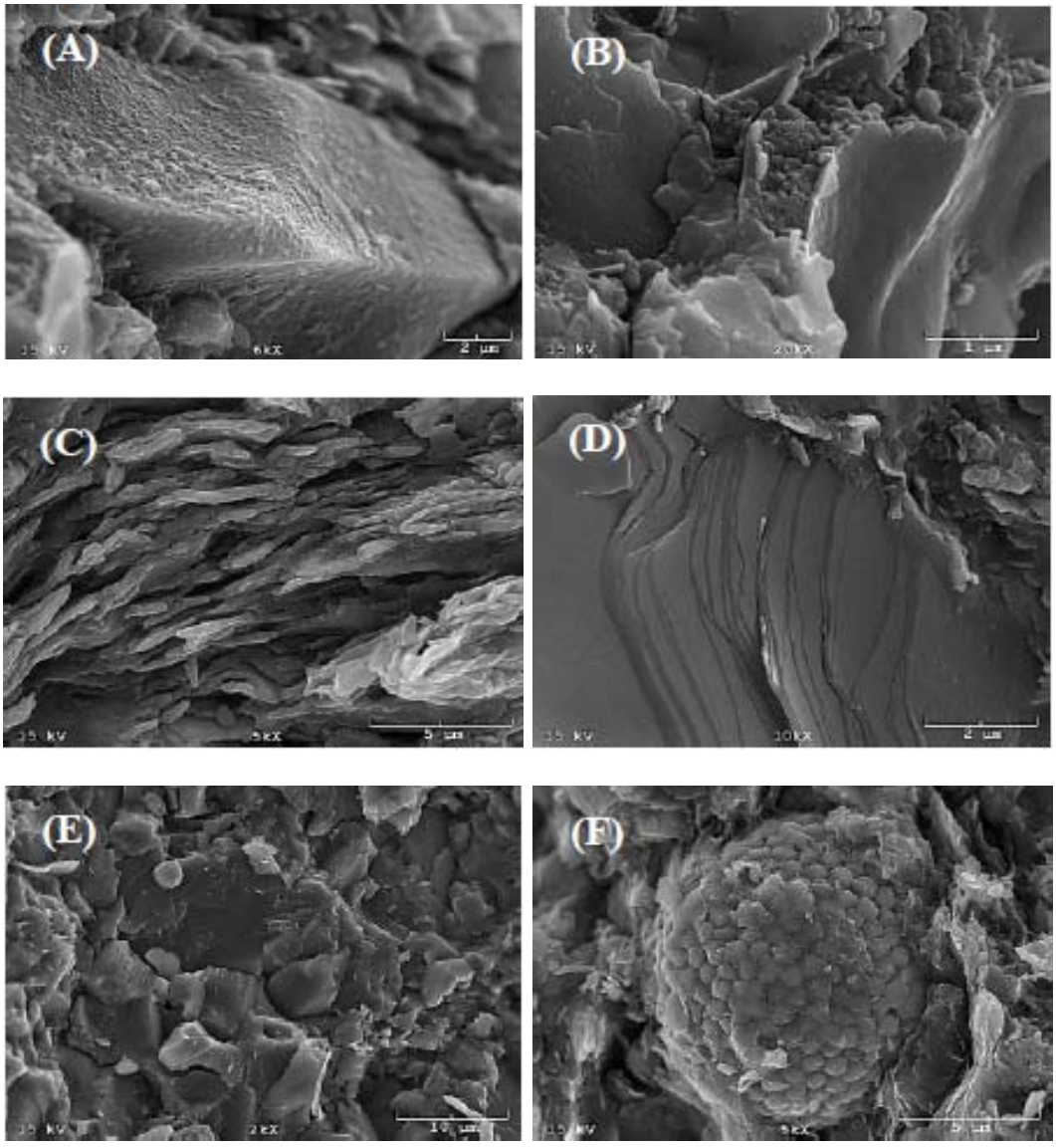

Figure 4.1: SEM pictures of common minerals in the natural gas shale. A) Detrital Quartz; B) Quartz Cement; C) Clay Mineral; D) Mica; E) Calcite; and F) Pyrite Framboids (Metwally and Chesnokov, 2011)

To facilitate the model to get referral input data and make the most effort to ensure the model's accuracy, FIB-SEM techniques are used to images minerals, pores, tiny channels and their connectivity, differentiate organic and inorganic phases, etc. (Metwally and Chesnokov, 2011).

Different minerals are found in the Barnett Shale (Figure 4.1). The samples are mainly comprised of quartz, clay minerals, pyrite, carbonate, etc. Every sample has a different amount, which matches with the XRD analysis.

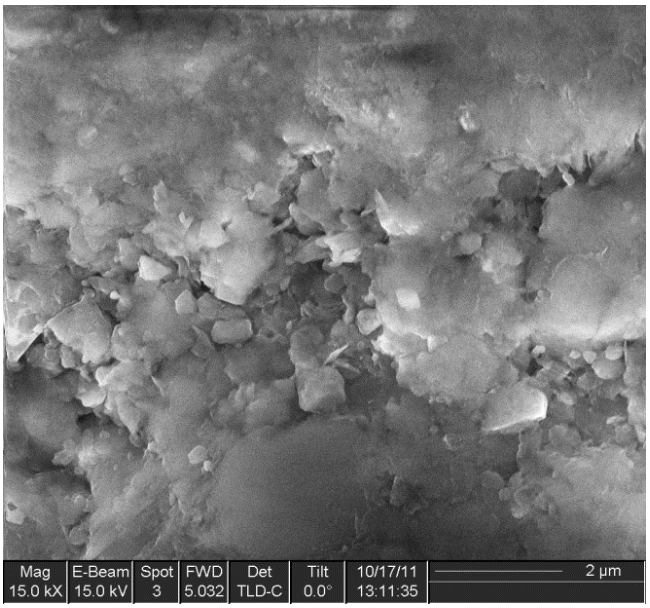

Figure 4.2: Quartz group

Moreover, there is a certain amount of organic matter, found in the kerogen, found by FIB-SEM (Figure 4.2), as well as some considerable porosity within the kerogen. The thermal maturity of the sample is within the gas window. It is plausible that there is storage of natural gas within it.

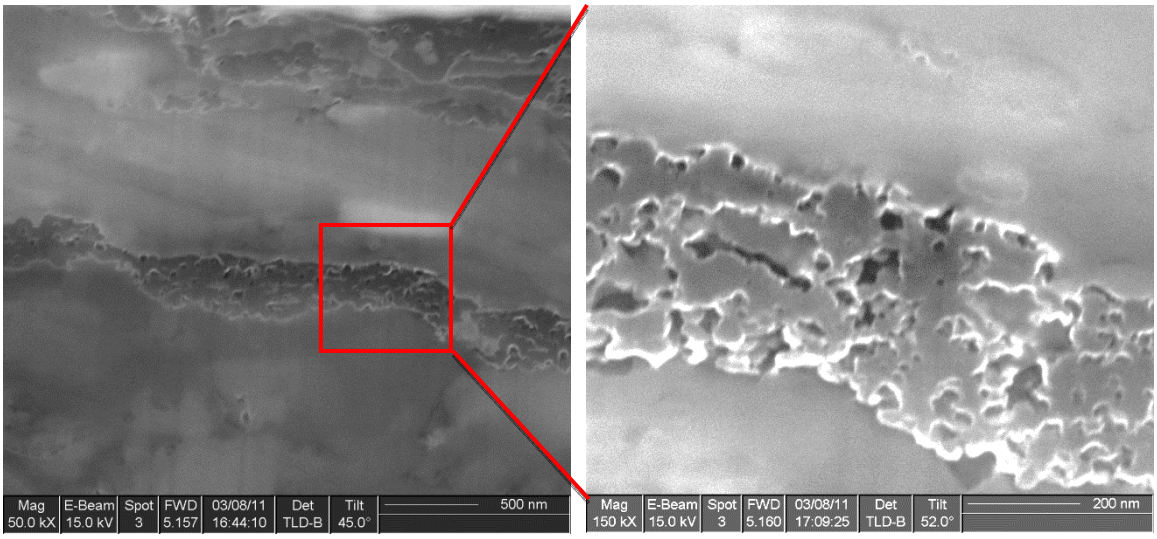

Figure 4.3: Organic matter, as found in kerogen, is imaged by FIB-SEM, with no alternation.

Carbonate and quartz pores are the most abundant pores in the Barnett Shale sample (Figure 4.3). This matches with the XRD results, which indicates that quartz is the most abundant mineral when compared to clay and carbonate, in the Barnett Shale.

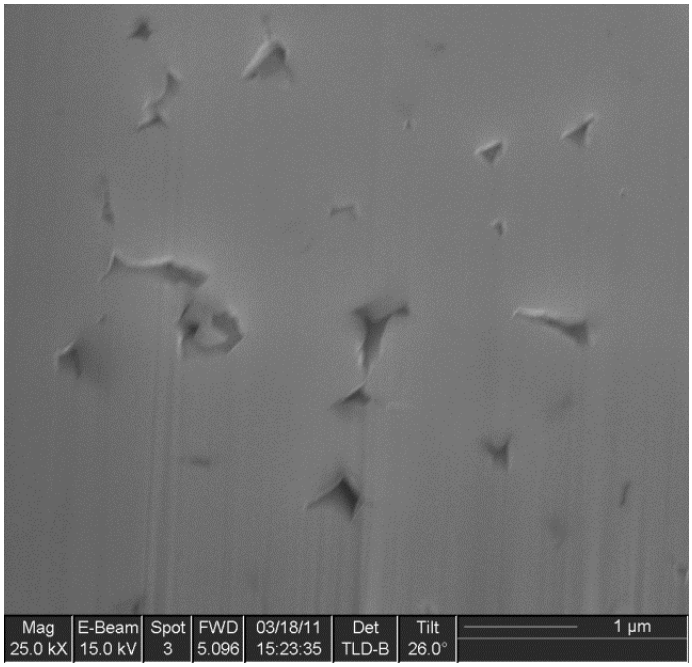

Figure 4.4: Inorganic (carbonate) pores

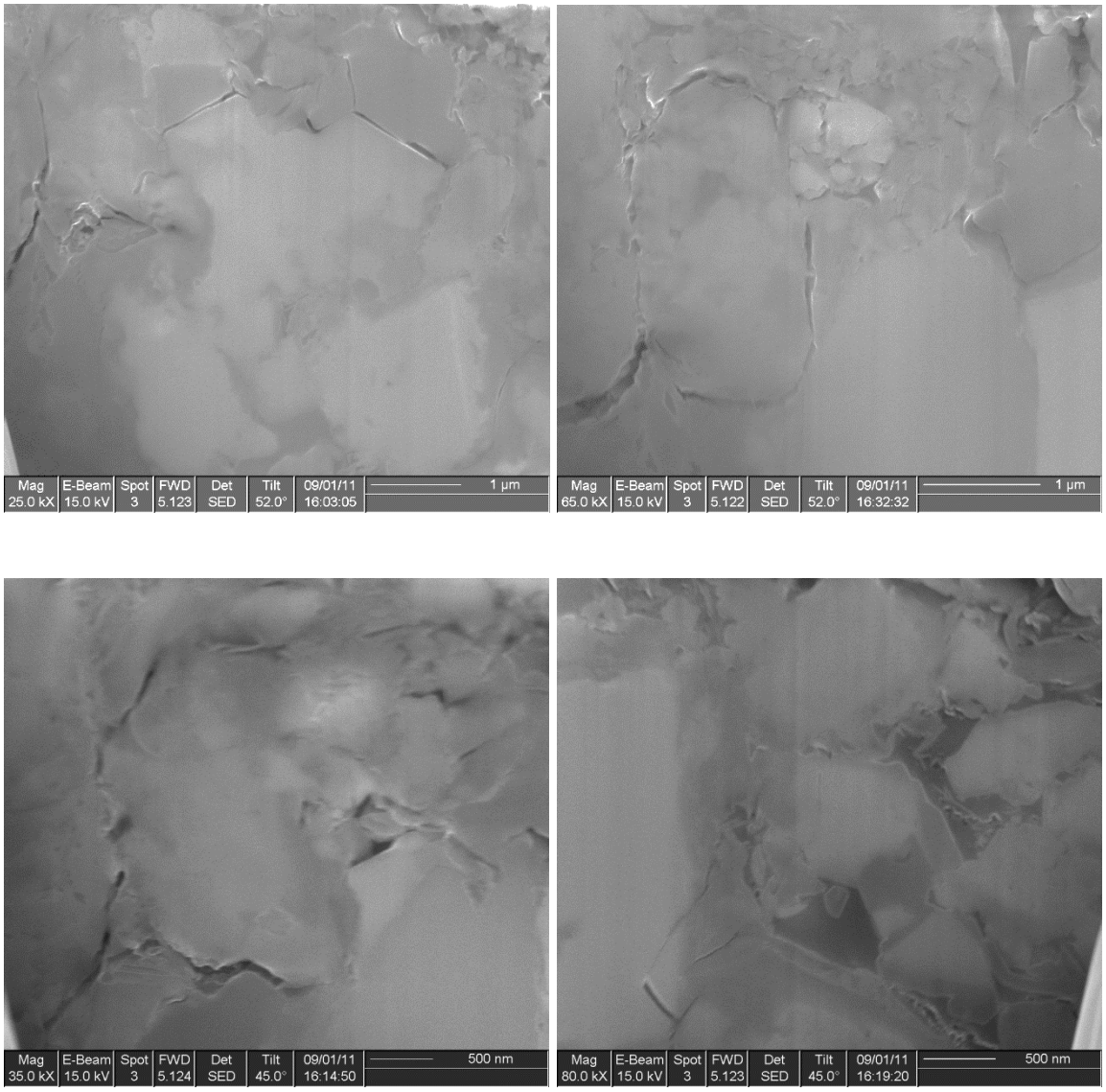

Figure 4.5: Tiny channels are found by FIB-SEM.

The above figures show the tiny channels with high aspect ratio found by FIB-SEM. Each of them has the same scale bars, 1µm and 500nm, respectively.

Based on the three above figures (Figure 4.3, 4.4, 4.5), a brief conclusion about the porosity in Barnett Shale could be drawn here, since the porosity is one of the critical inputs of the elasticity calculation model. Essentially, rock is assumed to have matrix

porosity (ϕM) and inclusion porosity (ϕI). Thus, ϕM could be estimated through those crack-like pores (Figure 2.1) and carbonate pores (Figure 4.4). Certain software may be helpful in finding the calculation of ϕM, such as Image J, etc.

Yet, there may be some crack-like pores induced by coring or sample preparation, rather than an in situ feature, and it may be worse for the cracks' connectivity on a larger scale (Heath, et al., 2011).

On the other hand, ϕI is considered as the porosity in organic matters (Figure 4.3). With the help of serial sectioning of FIB-SEM, all the cross-sectioned images in one area of interest can be stacked together, and then a 3D reconstruction of the sample is built. This 3D reconstructed cube provides not only a qualitative analysis of the internal connectivity of gas shale, but also a quantitative estimation of the % kerogen by volume, porosity, and etc. (Curtis, et al., 2010).

4.1.2 Advantages and Disadvantages of FIB-SEM

There are several ways to polish the sample surface, such as hand-made polishing and ion milling. However, compared to the former, ion milling would not have problems with the differential polishing, caused by the heterogeneity of gas shale. It is the electromagnetic lenses and scan coils focus and direct ions beam that make the promise of precise milling (Curtis, et al., 2010). Similar to FIB, another ion milling method uses a broad Ar^+ ion beam to remove the staff away from the surface via momentum transfer. This method is usually called BIB (Broad Ion Beam) milling. However, the accuracy of BIB milling is far less than that of FIB milling (Curtis, et al., 2010).

Some of the disadvantages are discussed as followed.

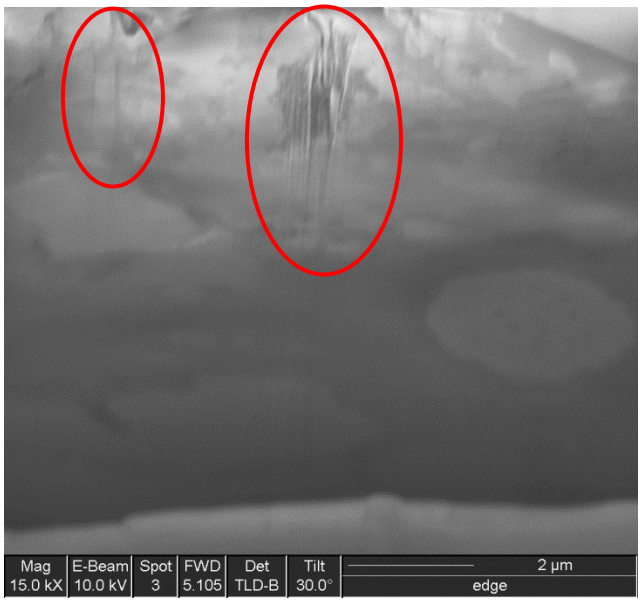

Figure 4.6: The red lines circle the curtaining artifacts when we do the milling on the Barnett Shale surface without deposition of Pt.

First of all, Figure 4.6 shows the curtaining effects caused by the milling process. Yet, it does have the possibility of making the interpreter consider the curtaining lines to be cracks in-situ. However, because of the high temperature and pressure, there is still a chance to melt the different sample surfaces, as the degree of melting changes with different properties of samples' materials.

Secondly, specimen charging, seen as bright visible spots in the images, is occasionally one of the hindrances to imaging artifacts. However, it happens often when processing the Barnett Shale, since it is organically rich (Heath et al., 2011).

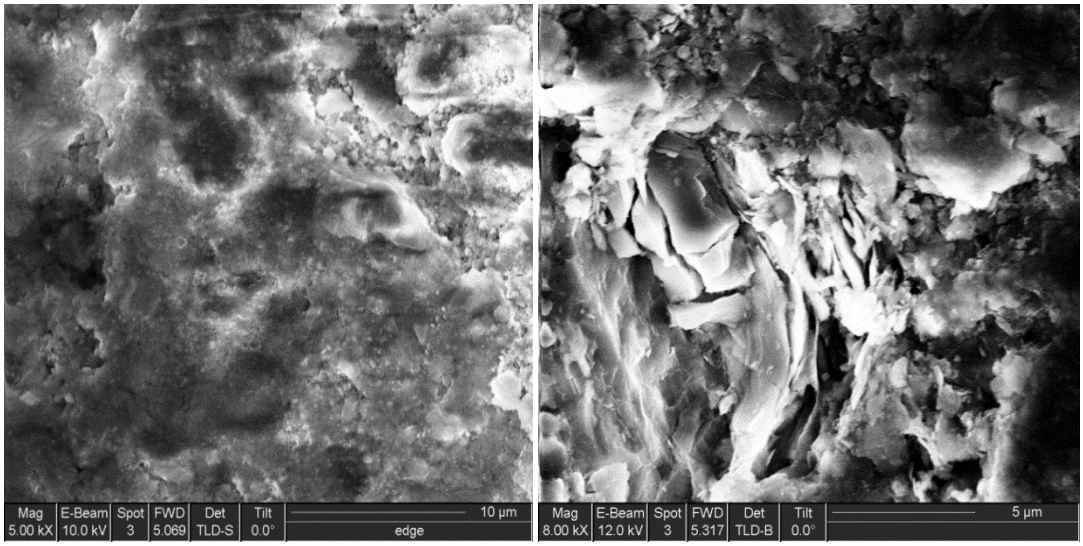

Figure 4.7: Charging effects (bright spots) on organic rich Barnett Shale sample.

Thirdly, there is another prevalent blemish to be seen in most of the FIB-SEM images, caused by mechanical cutting and rough polishing (Curtis, et al., 2010). The induced pores, circled in Figure 4.8, have no representative meaning of those deeper in the cross-sectional images. They could be used to tell the man-made pores apart from the natural ones, based on the obvious difference in shapes.

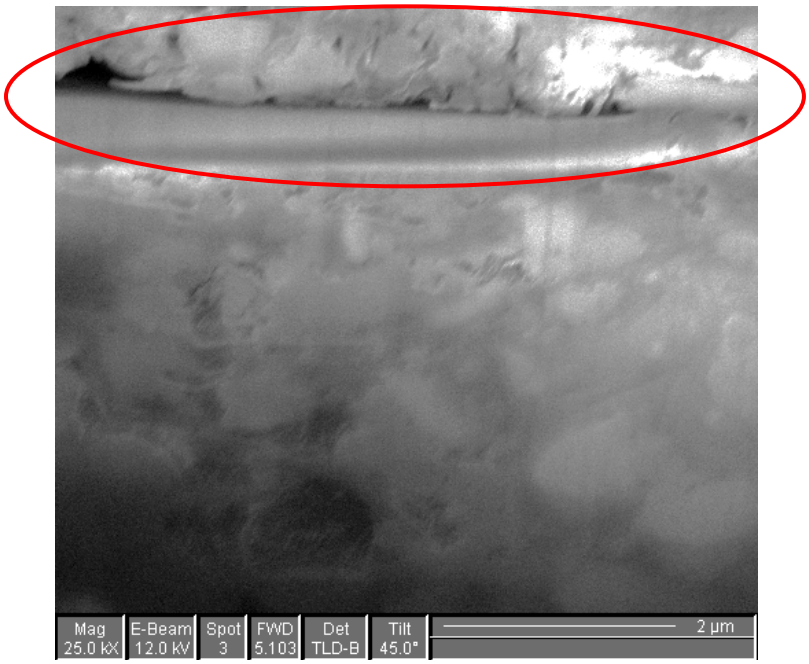

Figure 4.8: Undesired cracks created by FIB-SEM.

4.2 TOC Results and Discussion

It took almost 6 days to finish the experiments. The original results for the 12 core samples are shown below (See Table 3.2).

Table 4.1: The original TOC results of 12 core samples from Barnett Shale

NAME	MESS	CARBON (wt%)	SULFUR (wt%)	MEASURING TIME(s)
SC(i)	0.0905g	3.91	1.48	58
SC(ii)	0.0900g	4.76	1.18	87
JR(iii)	0.0900g	2.87	0.747	55
JR(iv)	0.0903g	2.54	2.11	67
AS(v)	0.0901g	0.80	0.198	203
AS(vi)	0.0900g	5.13	1.61	58
BR(vii)	0.0905g	3.60	1.05	87
BR(viii)	0.0908g	0.119	1.17	73
ST(ix)	0.0903g	5.93	1.53	55
ST(x)	0.0900g	5.80	1.61	83
RCT(xi)	0.0900g	2.84	0.743	108
RCT(xii)	0.0900g	3.48	1.15	55

Figure 4.9 generally shows the basic relationship between each set of samples. The red blocks are carbon, while the yellow ones are sulfur.

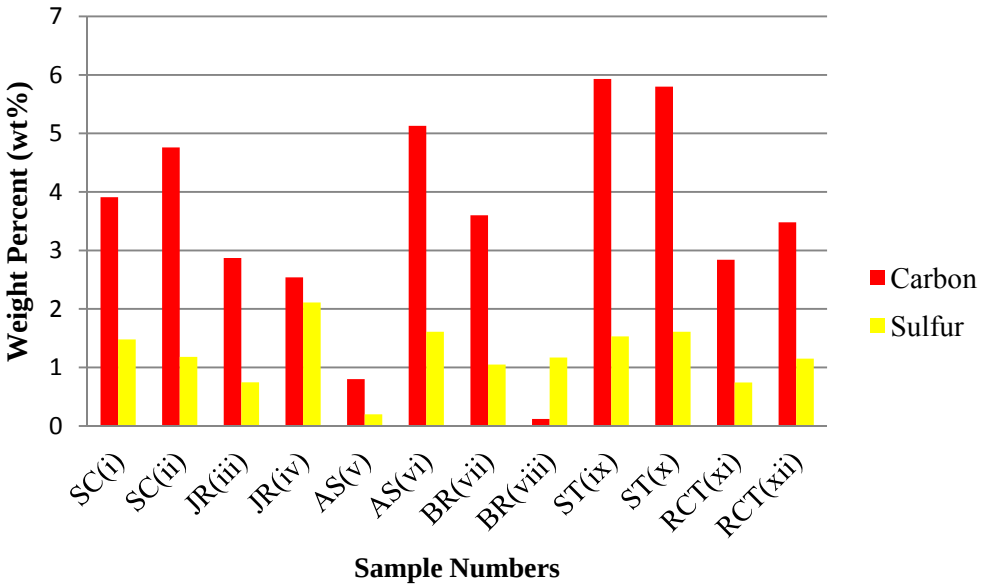

Figure 4.9: TOC wt% Results of 12 Barnett Shale samples

The results show that the maximum TOC among these 12 samples is up to 5.93% corresponding with sample ST(ix). However, the lowest value is as low as 0.119% derived from sample BR(viii). Overall, the average TOC value of the entire 12 samples is around 4%. Taking into consideration the Cl^- during the measurement, the correction is made out of necessity.

4.3 XRD Results Analysis

Apparently, the mineral content is a key factor indicating the best wells. Among the productive ones, the best production of Barnett Shale reservoirs comes from the areas composed by 45 wt% of quartz and only 27 wt% of clay (Bowker, 2003).

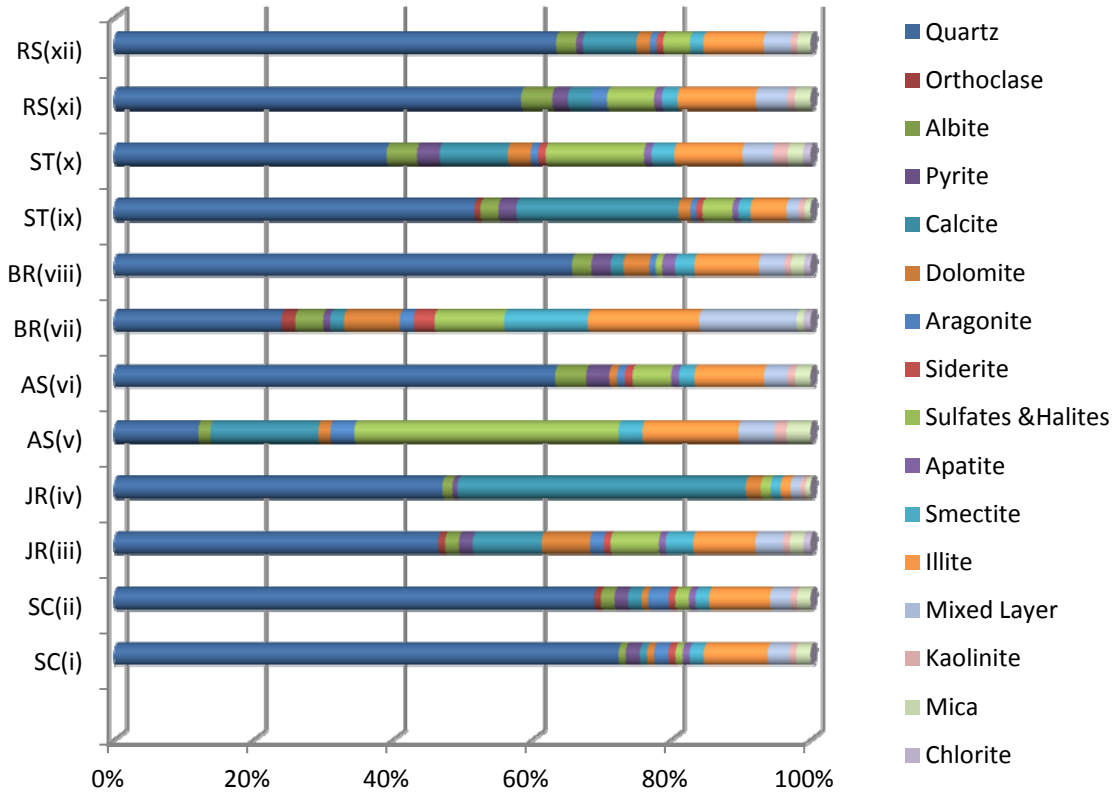

Figure 4.10: Mineral composition results of 12 Barnett Shale samples

12 sets of samples were measured. Results show in Figure 4.10, in Barnett Shale, quartz, calcite, and clay minerals, mostly illite, are the most abundant. Nevertheless, orthoclase, apatite, pyrite and siderite are the second most abundant minerals compared to the others (Metwally and Chesnokov, 2011).

Chapter 5:

Conclusions

Recently, the investigations of low-permeability geologic samples using FIB-SEM have been focused on defining and describing micrometer-scale pore types, morphology, capillarity, fractal scaling, and fluids in pores (Heath, et al., 2011). It has been verified that there will be no damage or exchange on the microstructure of the Barnett Shale during the FIB milling process (Curtis, et al., 2010).

Therefore, the suggestion could be made that for the microstructure study of gas shale, the FIB-SEM is one of the most powerful tools to cross-section the surface and save the images, since the channels and cracks within the gas shale are extremely tiny, or even on the nano-level. Moreover, the organic matter, found in kerogen, could be detected by this facility as well. Though there are still some other disadvantages, such as sample charging, etc., the FIB-SEM is still a reliable tool.

We found three different types of porosity in the Barnett Shale with the help of FIB - SEM, they are the cracks like, carbonate, and organic phased porosity. Also, there is grain-size dependent porosity between mineral particles. It can be done by the 3D reconstruction which means to create a 3D cube by stacking the images together.

The average TOC content for our 12 core samples is around 4~6%, which is not that high when compared to the other published values of gas shale reservoirs. For the mineral composition, the Barnett Shale core samples that we have are mainly composed of quartz and clay minerals dominated by calcite, illite, etc.

References

Aydemir, A., 2011, Comparison of Mississippian Barnett Shale, Northern-Central Texas, USA and Silurian Dadas Formation in Southeast Turkey: Journal of Petroleum Science and Engineering, p.81-93;

Barker, C., 1974, Pyrolysis Techniques for Source-Rock Evaluation: AAPG Bulletin, v. 58, no. 11, p. 2349-2361;

Bass, J., 1995, Minerals Physics and Crystallography: A Handbook of Physical Constants: AGU;

Bayuk, I., Ammerman, M., and Chesnokov, E., 2007a, Elastci Moduli of Anisotropic Clay: Geophysics, v. 72, p. D107-D117;

Bayuk, I., Ammerman, M., and Chesnokov, E., 2007b, Upscaling of Elastic Properties of Anisotropic Rocks: Journal of Geophysical International, v. 172, p. 842-860;

Belikov, B.P., Alexandrov, K., and Ryzhova, T.V., 1970, Elastic Properties of Rock Forming Minerals and Rocks: Nauka Publishers (in Russian);

Brooks, P.W., A.F. Embry, F. Goodarzi, and R. Stewart, 1992, Organic Geochemistry and Biological Marker Geochemistry of Schei Point Group (Triassic) and Recovered Oils from the Sverdrup Basin (Arctic Islands, Canada): Bulletin of Canadian Petroleum Geology, v. 40, p. 173-187;

Brooks, J., C. Cornford, and R. Archer, 1987: The Role of Hydrocarbon Source Rocks in Petroleum Exploration: Marine Petroleum Source Rocks; Edited by: Brooks, J. and Fleet, A. J.: Geological Society Special Publication, v. 26, p.17-48;

Bowker, K.A., 2003, Recent Development of the Barnett Shale Play, Fort Worth Basin: West Texas Geological Society Bulletin, v. 42, no. 6, p.1-11;

Chalmers, G., R. M. Bustin, and I. Powers, 2009, A Pore by Any Other Name Would be as Small: The Importance of Meso- and Microporosity in Shale Gas Capacity: Presented at the AAPG Annual Convention and Exhibition, Denver, CO;

Cope, M. J., 1981, Products of Natural Buming as a Component of the Dispersed Organic Matter of Sedimentary Rocks: Organic Maturation Studies in Fossil Fuel Exploration; Edited by: Brooks, J., Academic Press, London and New York, p. 89-109;

Curtis, M. E., R. J. Ambrose, C. H. Sondergeld, C. S. Rai, 2010, Structural Characterization of Gas Shale on the Micro- and Nano-Scales, Society of Petroleum Engineers, SPE Paper no. 137693, no. of pages: 15;

Energy from Shale, 2010, http://www.energyfromshale.org/barnett-shale-gas;

Hartfield, C., 2010, FIB Incidence Angles Impact Lift-Out Sample Success: Omniprobe's FIB and SEM Blog, http://info.omniprobe.com/Blog/bid/43133/FIB-Incidence-Angles-Impact-Lift-Out-Sample-Success;

Heath, J. E., T. A. Dewers, B. J.O.L. Mcpherson, R. Petrusak, T. C. Chidsey, A. J. Rinehart, and P. S. Mozley, 2011, Pore Networks in Continental and Marine Mudstones: Characteristics and Controls on Sealing Behavior: Geosphere, v. 7, p.429-454;

Holtzer, L., F. Indutnyi, P. H. Gasser, B. Munch, and M. Wegmann, 2004, Three-dimensional Analysis of Porous BaTiO3 Ceramics Using FIB Nanotomography: Journal of Microscopy, v. 216, p.84-95;

Jarvie, D. M., R. J. Hill, T. E. Ruble, and R. M. Pollastro, 2007, Unconventional Shale-gas Systems: The Mississippian Barnett Shale of North-Central Texas as One Model for Thermogenic Shale-Gas Assessment: AAPG Bulletin, v. 91, p.475-499;

Jarvie, D. M., R. J. Hill, T. E. Ruble, and B. M. Jarvie, in press, Unconventional Shale-Gas Resource Systems: Rocky Mountain Association of Geologists, CD-ROM；

Katahara, K., 1996, Clay Minerals Elastic Properties: SEG Expanded Abstract, v. 15, p. 1691-1694;

Metwally, Y. M. and E. M. Chesnokov, 2011, Gas Shale: Relationship between Permeability and Intrinsic Composition: SEG Expanded Abstract, v. 30, p. 4414-4419;

Montgomery, S. L., D. M. Jarvie, K. A. Bowker, and R. M. Pollastro, 2005, Mississippian Barnett Shale, Fort Worth Basin, North-Central Texas: Gas-Shale Play with Multitrillion Cubic Feet Potential: AAPG Bulletin, v. 89, no. 2, p. 155-175;

Nunez-Betelu, L. and J. I. Baceta, 1994, Basics and Application of Rock-Eval/TOC Pyrolysis: an Example from the Uppermost Paleocene/Lowermost Eocene in the Basque Basin, Western Pyrenees: Munibe Ciencias Naturales, v. 46, p. 43-62 (in Spanish and English);

Peselnick, L. and R. Robie, 1962, Elastic Constants of Calcite: Journal of Applied Physics, v. 33, p.34-36;

Pollastra, R., R. Hill, T. A. Ahlbrandt, R. R. Charpentier, T. A. Cook, T. R. Klett, and C. J. Schenk, 2003a, Assessment of Undiscovered Oil and Gas Resources of the Bend Arch – Fort Worth basin Province of North – Central Texas and Southwestern Oklahoma: USGS Fact Sheet, FS-2004-3022, http://pubs.usgs.gov/fs/2004/3022/fs-2004-3022.html;

Pollastro, R., R. J. Hill, D. M. Jarvie, and M. E. Henry, 2003b, Assessment Undiscovered Resources of the Barnett – Paleozoic Total Petroleum System, Bend Arch – Fort Worth basin Province, Texas: Online adaptation of presentation at AAPG Southwest Section Meeting, Fort Worth, TX., www.southwestsection.org;

Pollastro, R. M., D. M. Jarvie, R. J. Hill, and C. W. Adams, 2007, Geologic framework of the Mississippian Barnett Shale, BarnettPaleozoic total petroleum system, Bend Arch – Fort Worth Basin, Texas: AAPG Bulletin, v. 91, no. 4, p. 405-436.

Railroad Commission of Texas, 2012, http://www.rrc.state.tx.us/barnettshale/ index.php;

Rowe, H. D., R. G. Loucks, S. C. Ruppel, and S. M. Rimmer, 2008, Mississippian Barnett Formation, Fort Worth Basin, Texas: Bulk Geochemical Inferences and Mo-TOC Constraints on the Severity of Hydrographic Restriction: Chemical Geology, v. 257, p.16-25;

Schieber, J., 2010, Common Themes in the Formation and Preservation of Intrinsic Porosity in Shale and Mudstones – Illustrated with Examples across the Phanerozoic: Society of Petroleum Engineers, SPE Paper no. 132370, no. of pages: 10;

Schmoker, J. W., 2002, Resource-Assessment Perspectives for Unconventional Gas Systems: AAPG Bulletin, v. 86, no. 11, p.1993-1999;

Stanjek, H. and W. Haulser, 2004, Basis of X-Ray Diffraction: Hyperfine Interactions, v. 154, p.107–119;

Tiwary, K. D., 2007, Mathematical Modeling and Ultrasonic Measurement of Shale Anisotropy and a Comparision of Upscaling Methods from Sonic to Seismic, University of Oklahoma, PhD. Dissertation, no. of pages: 198;

Tolke, J., C. Baldwin, Y. Mu, N. Derzhi, Q. Fang, A. Grader, J. Dvorkin, 2010, Computer Simulations of Fluid Flow in Sediment: from Images to Permeability: the Leading Edge, v. 29, p.68-74;

Tomustsa, L. and D. Silin, 2004, Nanoscale Pore Imaging and Pore Scale Fluid Flow Modeling in Chalk, Lawrence Berkeley National Laboratory: Lawrence Berkeley National Laboratory, http://escholarship.org/uc/item/9b86t01t;

Tomustsa, L., D. Silin, and V. Radmilovic, 2007, Analysis of Chalk Petrophysical Properties by Means of Submicron-Scale Pore Imaging and Modeling: SPE Reservoir Evaluation & Engineering, v. 10, Issue 3, p. 285-293;

U.S. Energy Information Administration, 2010 and 2011, http://www.eia.gov/ naturalgas/;

U.S. Geological Survey, 2010, http://www.usgs.gov/;

Wang, F. P. and R. M. Reed, 2009, Poor Networks and Fluid Flow in Gas Shales: Society of Petroleum Engineers, SPE Paper no. 124253, no. of pages: 8;

Waples, D. W., and R. W. Marzi, 1979, The Universality of the Relationship between Vitrinite Reflectance and Transformation Ratio: Organic Geochemistry, v. 28, no. 6, p. 383-388.